Temperature and mineral dust variability recorded in two low accumulation Alpine ice cores over the last millennium

Pascal Bohleber[1,2,3], Tobias Erhardt[4,5], Nicole Spaulding[1], Helene Hoffmann[2], Hubertus Fischer[4,5], and Paul Mayewski[1]

[1]Climate Change Institute, University of Maine, Orono, Maine, USA
[2]Institute of Environmental Physics, Heidelberg University, Heidelberg, Germany
[3]Institute for Interdisciplinary Mountain Research, Austrian Academy of Sciences, Innsbruck, Austria
[4]Climate and Environmental Physics, Physics Institute, University of Bern, Bern, Switzerland
[5]Oeschger Centre for Climate Change Research, University of Bern, Bern, Switzerland

Correspondence to: Pascal Bohleber (Pascal.Bohleber@iup.uni-heidelberg.de)

Abstract. Among ice core drilling sites in the European Alps, Colle Gnifetti (CG) is the only non-temperate glacier to offer climate records back to at least 1000 years. This unique long-term archive is the result of an exceptionally low net accumulation driven by wind erosion and rapid annual layer thinning. However, the full exploitation of the CG time series has been hampered by considerable dating uncertainties and the seasonal summer bias in snow preservation. Using a new core drilled in 2013 we extend annual layer counting, for the first time at CG, over the last 1000 years and add additional constraints to the resulting age scale from radiocarbon dating. Based on this improved age scale, and using a multi-core approach with a neighboring ice core, we explore the time series of stable water isotopes and the mineral dust proxies Ca^{2+} and insoluble particles. Also in our latest ice core we face the already known limitation to the quantitative use of the stable isotope variability based on a high and potentially non-stationary isotope/temperature sensitivity at CG. Decadal trends in Ca^{2+} reveal substantial agreement with instrumental temperature and are explored here as a potential site-specific supplement to the isotope-based temperature reconstruction. The observed coupling between temperature and Ca^{2+}-trends likely results from snow preservation effects and the advection of dust-rich air masses coinciding with warm temperatures. We find that if calibrated against instrumental data, the Ca^{2+}-based temperature reconstruction is in robust agreement with the latest proxy-based summer temperature reconstruction, including a "Little Ice Age" cold period as well as a medieval climate anomaly. Part of the medieval climate period around 1100–1200 AD clearly stands out through an increased occurrence of dust events, potentially resulting from a relative increase in meridional flow and/or dry conditions over the Mediterranean.

1 Introduction

Glaciers and ice caps of high mountain ranges can provide climate records of mid- and low latitudes complementary to polar ice cores. In comparison to their polar counterparts, mountain drilling sites are characterized by a comparatively small-scale glacier geometry and their proximity to continental source areas. As a consequence, cold mountain glaciers are an especially worthwhile target for ice core studies focusing on Holocene climate, e.g. in view of the envisaged IPICS 2k array (Brook et al.,

2006) and the present underrepresentation of ice core records contributing to the PAGES 2k Network (Ahmed et al., 2013). In the European Alps, ice core studies have been performed at Col du Dôme, Mont Blanc (Preunkert et al., 2000), Fiescherhorn, Bernese Alps (Schwerzmann et al., 2006), Ortles, Eastern Alps (Gabrielli et al., 2016) as well as at Colle Gnifetti and Colle del Lys in the Monte Rosa region (e.g. Wagenbach et al., 2012, and references therein). Among these glaciers, Colle Gnifetti

5   (CG) – in spite of its limited glacier depth – stands out as the only non-temperate site where net snow accumulation is low enough to provide records over the last millennium and potentially beyond at a reasonable time resolution. The exceptionally low net accumulation at CG is a result of seasonal net snow loss by wind erosion: Since snow consolidation is most effective during the summer half year, winter precipitation is more likely to be removed from the surface (Wagenbach, 1992). This has far-reaching consequences with respect to the interpretation of the CG ice cores, hampering to-date the full exploitation of their

10   unique long climate time series. On the one hand, considerable uncertainty in the individual ice core chronologies becomes an obstacle already after a few hundred years. Difficulties in deploying annual layer counting as the main dating tool arise from snow scouring, rapid layer thinning associated with strongly non-linear time-depth relationships and the extremely low time resolution achieved in the bottom part of the glacier by conventional cm-resolution analyses. As a consequence, dating the deeper part of CG ice cores is commonly based on simple extrapolation combined with constraints from radiocarbon analysis

15   (e.g. Jenk et al., 2009). On the other hand, irregular and summer-biased snow deposition makes the annual or long-term levels of ice core proxy signals with a prominent seasonal cycle a primary function of the relative winter snow fraction preserved, as opposed to their common climatological meaning. In addition, net snow accumulation is characterized by substantial spatial and temporal variability, leading to considerable influence of upstream flow effects and depositional noise (Wagenbach, 1992). In contrast to the strong signals of anthropogenic aerosol increase, depositional noise especially challenges the detection of the

20   comparatively weak stable water isotope trends (δ^{18}O and δD). Under these circumstances, the comparison of multiple cores drilled at the same site can be used to identify an atmospheric signal as shared variability among the cores (Bohleber et al., 2013; Wagenbach et al., 2012).

Here we present new results to tackle the two-fold challenge above with a new core drilled at Colle Gnifetti in 2013, integrating datasets from an additional ice core drilled in 2005 on the same flow line. In order to obtain a reliable long-term chronology for

25   the 2013 core, we utilize state-of-the-art continuous flow analysis for ice core impurity profiling and, to identify even highly thinned annual layers, laser ablation inductively coupled plasma mass spectrometry (LA-ICP-MS) at sub-mm depth resolution (Della Lunga et al., 2017; More et al., 2017; Haines et al., 2016; Mayewski et al., 2014). We combine annual layer counting in the resulting impurity profiles with absolute age constraints from radiocarbon analysis, taking advantage of recent progress in applying this technique to mountain ice cores (Hoffmann et al., 2017b; Uglietti et al., 2016). Based on a refined long-term

30   chronology, the time series of stable water isotopes and mineral dust proxies (Ca^{2+} and insoluble particles) are investigated, with special emphasis on their relation to temperature.
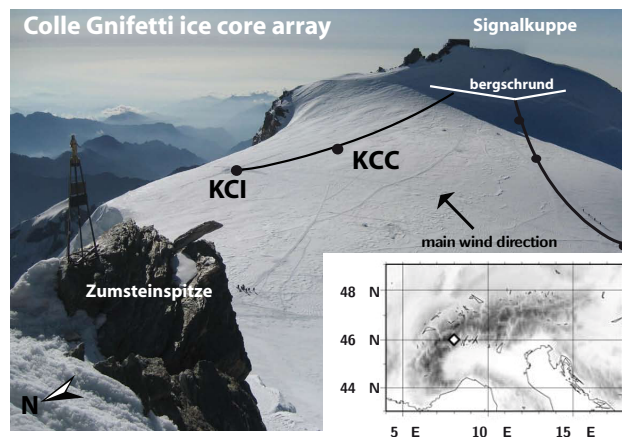
Figure 1. The ice core array at Colle Gnifetti, at 4450 m asl in the Monte Rosa summit range. The drilling sites of the two cores KCI and KCC are located on approximately the same flow line (black line) towards the eastern flank (downwind of the main wind direction), hence providing their same upstream catchment area. Locations of previous drillings initiated by the Institute of Environmental Physics are also shown as small black dots for reference.

2 Glaciological settings of the CG drilling site

Details on the glaciological features of CG are described thoroughly in the literature; e.g. Haeberli et al. (1988); Lüthi and Funk (2000); Konrad et al. (2013) for geometry and glacier flow, Haeberli and Funk (1991); Hoelzle et al. (2011) for englacial temperature and Alean et al. (1983) for surface accumulation. Here, we present only a brief overview, mainly dedicated to
5   explaining the role of snow deposition in relation to recording atmospheric temperature and mineral dust variability in the CG ice cores.

With a horizontal scale of 400 m and a maximum ice thickness of around 140 m, the CG site forms a small firn saddle at around 4500 m asl between two summits of the Monte Rosa massif. The orientation of the convex, central saddle axis coincides with the main westerly wind direction, thereby making the downwind-situated ice cliff a perfect sink for drifting snow
10   (Figure 1). Hence, a substantial fraction of the annual fresh snow precipitation is removed at CG, which limits linking the net snow accumulation rate to the climatologic precipitation rate. The latter ranges from 0.15 m water equivalent (WE) per year in the north-facing flank to about 1.2 m WE per year in the southern one, where the higher abundance of ice layers and ice crusts significantly reduces the snow erosion rate (Alean et al., 1983). Within the CG north flank (comprising our CG ice core array) fresh snow consolidation is faster during the summer half year (additionally supported by refreezing surface melt). Accord-
15   ingly, the mean net snow accumulation is mainly made up by precipitation of the warm seasons, which entails a systematic over-representation of the summer half-year in chemical and isotopic signatures (Wagenbach, 1989). A changing amount of winter precipitation contributing to annual mean values may introduce a coupling on the inter-annual scale among seasonal varying signals, including $\delta^{18}O$ and most impurities (Wagenbach, 1992). Notably this also includes a potential link to temper-

ature, since warm summers feature increased vertical mixing and hence a higher atmospheric impurity load. In addition, faster fresh snow consolidation favored by higher temperatures may lead to an increased relative amount of impurity-rich summer snow deposition.

A long-term co-variation between $\delta^{18}O$ and Ca^{2+} suggesting a possible relationship between climate and dust deposition at CG has already been noted but was left for future investigation (Wagenbach and Geis, 1989; Wagenbach et al., 1996). A later study specifically explored the link between the $\delta^{18}O$ signal and air temperature changes in the presence of the snow preservation influence at CG. A dominant influence of atmospheric temperature on decadal isotope variability shared among the CG cores was found, although a high and potentially non-stationary isotope/temperature sensitivity hampered the quantitative use of the CG isotope variability (Bohleber et al., 2013). Considering the co-variation of the long-term variability of i) Ca^{2+} and $\delta^{18}O$, and ii) $\delta^{18}O$ and temperature, suggests that atmospheric temperature variability could also be reflected in the Ca^{2+} trends. In view of the shortcomings in quantitatively using the isotope-thermometer at CG, identifying a temperature-related imprint in the Ca^{2+} variability could provide a valuable supplement in this respect.

At CG, mineral background aerosol levels are generally low, making the Ca^{2+} record is dominated by episodic inputs of dust, most likely originating in the Saharan desert (Wagenbach et al., 1996). While dry deposition may add to the average mineral dust content (Haeberli et al., 1983), it appears less important in case of Saharan dust events (Schwikowski et al., 1995). In addition, only a marginal contribution to changes in the particle size distribution is expected from changes in the dry deposition (Ruth et al., 2003). As for most of the impurity species at CG, the seasonal contrast in Ca^{2+} concentration is primarily connected to the seasonal gradient in vertical atmospheric mixing, with an additional component from sporadic Saharan dust inputs (Preunkert et al., 2000; Preunkert and Wagenbach, 1998). Saharan dust deposition events are a frequent phenomenon in the Alps with main occurrence in spring and summer (Prodi and Fea, 1979). A single deposition event typically lasts less than a few days (Sodemann et al., 2005; Schwikowski et al., 1995). The associated warm air temperature and the substantially lowered snow albedo both support surface snow consolidation and partly protect the dust layer from wind erosion (Haeberli et al., 1983). Intensive Saharan dust events of the summer half year, associated with directly northward transport of air masses, are most likely to become preserved at CG. Saharan dust layers in CG ice cores can be characterized by high concentrations of insoluble particles, SO_4^{2-} and Ca^{2+} coinciding with buffered low acidity, as well as to some extent by increased $\delta^{18}O$ and deuterium excess values (Wagenbach et al., 1996; Wagenbach and Geis, 1989). Accordingly, the combination of Ca^{2+} with an alkalinity measurement is a specific tool to identify Saharan dust influenced layers in CG ice cores (Wagenbach et al., 1996), which will be employed in the following.

The above considerations warrant a general distinction and separate evaluation of the following two features of the Ca^{2+} record of the CG ice cores: i) The long-term average Ca^{2+} concentration, and its potential coupling with $\delta^{18}O$ and temperature via snow preservation. ii) Spikes in Ca^{2+} typically two orders of magnitude above background, which are dominated by Saharan dust input (Wagenbach et al., 1996). Regarding ii), changes in the dust peak occurrence rate can originate from changes in the meridional versus zonal circulation and/or in the desert dust source strength. Here detecting the frequency of dust peaks in the ice core matters, which is expected to be comparatively more robust against snow preservation influence.

Table 1. Basic glaciological parameters of the two CG ice cores

Core name	KCI	KCC
Position GPS (WGS84)	N 45.92972 E 7.87696	N 45.92893 E 7.87627
Year of drilling	2005	2013
Total depth [m abs]	61.84	71.81
Total depth [m WE]	48.44	53.77
Surface net accumulation [cm WE/yr]	14	22
Firn-ice-transition [m WE]	17	21

3 Ice core analysis

The two cores used in this study, denoted as KCI and KCC, were drilled in 2005 and 2013, respectively. Both cores were drilled roughly on the same flow line, making them the natural choice for our inter-core comparison, i.e. opposed to using previously deep cores drilled on another flow line (Figure 1). Table 1 summarizes basic glaciological parameters of the two cores. The depth sections used in this study were chosen to comprise roughly the last 1000 years, i.e., the upper 44 m WE (corresponding to 81% relative depth) and 35 m WE (73% relative depth) of KCC and KCI, respectively. Table 2 provides an overview of the carefully co-registered datasets used in this study. The various methods of analysis are discussed briefly in the following.

3.1 Impurity profiles from continuous flow analysis

Continuous flow analysis (CFA) of the KCC core was performed with the setup at the Division for Climate and Environmental Physics, Physics Institute, at the University of Bern. Analyses performed on the meltwater flow included meltwater conductivity, insoluble particle concentration and size distribution as well as selected ion species (Ca^{2+}, NH_4^+, NO_3^-, Na^+, see Table 2). In addition, stable water isotopes were analyzed using a Picarro instrument coupled directly to the meltwater flow. The size distribution of insoluble particles recorded by the optical particle sensor was used to derive a profile of the "coarse particle percentage" (CPP). The CPP was calculated based on particle volume, and represents the percentage of particles exceeding a threshold of 4.0 μm. The threshold was chosen such that it corresponds to the expected median particle diameter of Saharan dust particles at CG, which was shown to be distinguishable from background sources (Wagenbach and Geis, 1989). Deviations from a CPP of 50% indicate higher or lower contribution of large and small particles respectively. The melt rate was adjusted to provide the necessary amount of water for all analyses resulting in an effective depth resolution ranging from 1.2 cm at the very top of the core to about 0.5 cm for all depth below approximately 25 m WE. Electrical conductivity measurements (ECM) performed at the Institute of Environmental Physics, Heidelberg University were used primarily to obtain a qualitative record of the acidity of the ice in connection to the detection of Saharan dust events.

The KCI core was analyzed using the reduced CFA setup at the Institute of Environmental Physics, Heidelberg University. Meltwater conductivity and insoluble particle concentration were measured by CFA at about 0.7 cm effective resolution. Con-

Table 2. Overview on ice core analyses and datasets used in this study

Core	Parameters	Sampling	Effective resolution [cm]
KCC	Meltwater Conductivity, NH_4^+, NO_3^-, Na^+	Continuous Flow	> 0.5
	Insoluble Particles, Ca^{2+}	Continuous Flow	> 0.5
	Stable water isotopes ($\delta^{18}O$ and δD)	Continuous Flow	> 0.5
	Electric Conductivity	ECM	> 0.5
	^{44}Ca	Laser ablation ICP-MS	$120\,\mu m$
KCI	Meltwater Conductivity, Insoluble Particles	Continuous Flow	> 0.7
	Stable water isotopes ($\delta^{18}O$ or δD)	Discrete Sampling	$10 - 1.5$

tinuous sub-sampling of the core for stable water isotope analyses was conducted at a depth resolution typically ranging between 5 and 10 cm. Due to the relatively high firn temperature at CG, isotope smoothing is much faster compared to polar sites with similar annual layer thickness. Hence re-sampling most of KCI even at 1.5 cm depth resolution did not significantly restore any high-frequency isotope variability (Bohleber et al., 2013).

3.2 Ultra-high resolution Ca-profile of the KCC core by laser ablation ICP-MS

Laser ablation inductively coupled plasma mass spectrometry (LA-ICP-MS) was conducted in the WM Keck Laser Ice Facility at the Climate Change Institute (University of Maine) and used to analyze ^{44}Ca at ultra-high depth resolution (better than $120\,\mu m$). The more abundant ^{40}Ca is blocked by mass interference from ^{40}Ar used as carrier gas. Details regarding the method, sample preparation and calibration routine can be found in Sneed et al. (2015). Briefly, the components of this system include a Thermo Element 2 ICP-MS, a New Wave UP-213 laser, and a cryo-cell chamber, designed to seal a 1 m ice core from the surrounding air while maintaining a uniform temperature of $-15°$ C. In order to ensure a complete seal of the ablation chamber, porous firn parts could not be measured. From 29.5 m WE to bedrock, the KCC ice core was analyzed for ^{44}Ca along a single ablation track. The ^{44}Ca signal comprises contributions of soluble and insoluble Ca (Sneed et al., 2015). Crucial for further deployment for annual layer counting, the trend components in the LA-ICP-MS measured Ca signal have been shown to be in good correspondence with the lower resolution CFA Ca signal, as shown in Figure 2 and previously by Sneed et al. (2015).

3.2.1 Radiocarbon analysis

The measurements for radiocarbon dating of the ice core have been conducted at the Institute of Environmental Physics (Heidelberg, Germany) under close collaboration with the accelerator mass spectrometer (AMS) facility at the Klaus-Tschira-Lab in Mannheim, Germany. The microscopic particulate organic carbon fraction (POC) incorporated into the ice matrix was extracted, combusted and analyzed for ^{14}C content. Calibration of the retrieved ^{14}C ages was performed using OxCal version 2.4
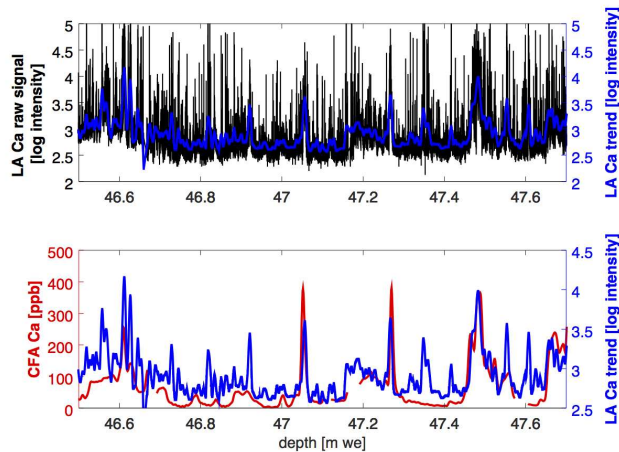
Figure 2. Ca signals obtained from the KCC ice core at around 65% relative depth using LA-ICP-MS and CFA in direct comparison after careful alignment of the two depth scales. Top row: Raw (black) and filtered LA-ICP-MS Ca signal (blue). Bottom: CFA Ca (red) vs filtered LA-ICP-MS Ca signal (blue). Note i) additional peaks and high-frequency information revealed by LA-ICP-MS, ii) a general agreement of CFA and low frequency LA-ICP-MS components is consistently observed over core parts measured by LA-ICP-MS. LA-ICP-MS intensity is reported as counts per second.

(Ramsey, 2016) and by convention the 1-sigma error range is shown (Stuiver and Polach, 1977). For details on the sample preparation and measurement procedure see Hoffmann et al. (2017a, b); Hoffmann (2016). The average ice sample masses were for both cores in a range of ca. 300–500 g ice resulting in absolute POC masses below 10 μgC. For the KCC core, a fraction of the ice core with a cross section of 17 cm^2 was reserved for the POC ^{14}C analysis. Within the upper 44 m WE, a total of six samples were analysed, typically comprising between 40–60 cm of core. For the KCI ice core more core material (one third) was available, resulting in depth intervals of 40 cm length used for radiocarbon dating. Within the upper 40 m WE of the KCI core five samples have been analyzed so far.

4 Ice core dating

Ice core chronologies were established by annual layer counting as the main dating tool in combination with additional age constraints from ^{14}C for the lower core parts. For roughly the last 100 years, dated time horizons (1963 bomb-radioactivity, and the Saharan dust layers of 1977, 1947 and 1901, cf. Figure 4 below) are available to constrain the counting (Table A1 with the depths of the respective horizons for KCC and KCI is included in the appendix). The 1963 horizon was used to cross-check that the annual signal had been identified correctly (cf. sub-annual and multi-year signals). The dust events were independently used for verification and typically lie within one to two years of the counted age scale (four years at maximum for the 1901 horizon). Regarding additional absolute age markers beyond 1901, the identification of volcanic eruptions solely based on basic ice chemistry profiles is not feasible at CG. This is due to the fact that the relatively weak signals of volcanic
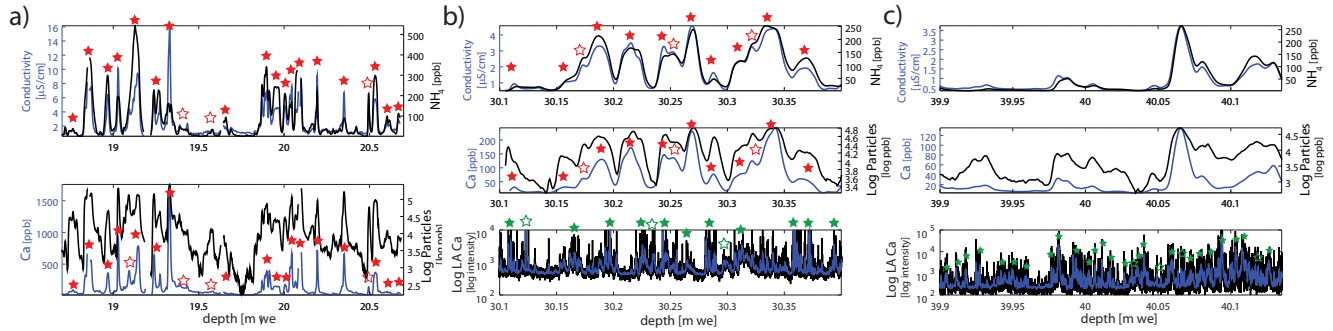
Figure 3. Examples for annual layer counting in KCC impurity profiles for three different depth sections, labeled a), b) and c), and corresponding roughly to 100, 250 and 1000 years before 2013, respectively (cf. Table 3). In the upper core parts (firn sections) CFA measured impurities were used for counting, with special emphasis on NH_4^+ (a). Counted years are marked as full stars, uncertain years as white stars. The middle row (b) shows an example of overlap in counting between CFA and LA-ICP-MS Ca, showing (10 ± 3) and (11 ± 3) years, respectively. The LA-ICP-MS Ca raw signal is shown in black together with Gaussian smoothing (blue). Note that a minor depth offset (at most a few cm) may exist between the CFA and LA-ICP-MS datasets. Accordingly, no one-to-one match of the individual peaks is attempted. Counting within one of the deepest sections analysed for this study is shown in (c). Here, only the LA-ICP-MS Ca allows a reliable identification of almost sub-cm thin annual layers. LA-ICP-MS intensity is reported as counts per second.

sulphate or volcanic acidity are easily overlooked at CG since they are embedded into the relatively large variability of Saharan dust associated sulphate (mainly from gypsum) and (acidity consuming) carbonate. More promising in this respect is the investigation of relatively volatile trace elements (Kellerhals et al., 2010b), or the detection of tephra markers, which are beyond the scope of this work, however.

4.1 The KCI chronology

For KCI, insoluble particle concentration and meltwater conductivity were used for annual layer counting, extending down to about 26 m WE. Below 26 m WE the identification of annual layers became ambiguous and was abandoned. This depth corresponds (taking the uncertainty in layer counting into account) to (1492 ± 30) AD. A two-parameter model (based on a simple analytical expression for the decrease of the annual layer thickness with depth) was used to extrapolate a continuous age-depth relation to greater depth (Nye, 1963; Jenk et al., 2009). Note that high-resolution annual layer counting could only be performed in KCC (see below) since only small sections of KCI have been analyzed by LA-ICP-MS so far (Sneed et al., 2015).

4.2 The KCC chronology

All impurity species measured by CFA (Table 2) were used in combination for annual layer counting. Annual layers were defined as local maxima in at least two of the six impurity signals, with special emphasis on NH_4^+ featuring the largest seasonal amplitude. An example of counting annual layers in the CFA profiles in shown in Figure 3 a). In order to identify highly

Table 3. Ice core age, dating uncertainty and annual layer thickness for selected depths

Core	Depth [m WE]	Age [year AD]	Uncertainty [years]	Annual Layer Thickness [cm WE]
KCC	10	1971	1	18
	20	1912	4	11.5
	30	1762	12	2.7
	40	1000	72	1
KCI	10	1917	4	7.4
	20	1700	20	3.2
	30	1312	62	1.7
	35	939	77	1

thinned, sub-cm annual layers expected to dominate the deeper core sections, an independent counting was established using the LA-ICP-MS Ca profile starting at 29.5 m WE (corresponding to 1760 AD). At this depth, the average annual layer thickness was estimated from CFA-based counting as around 3 cm. The LA-ICP-MS Ca record was investigated at full resolution and as a smoothed version (using the leading components in singular spectrum analysis or Gaussian smoothing). In its upper section,

5   the LA-ICP-MS Ca profile is characterized by regular occurrence of several distinct peaks grouped together going along with an elevated baseline of Ca concentration (Figure 3 b)). The groups of peaks are separated by a comparatively stable signal of low Ca concentrations. The latter is interpreted as resulting from the varying degree of winter snow being included in the record otherwise dominated by summer snow. Accordingly, the grouped peaks correspond to sub-annual snow deposition events of elevated Ca concentration during the summer period, which is also observed in the most shallow parts of KCC (see Figure

10   A1 in the appendix). For the depth interval 29.5–32.5 m WE, counting separated groups of peaks (typically 3–5 peaks per annual layer) in the LA-ICP-MS Ca record results in good agreement with counting performed on the CFA profile (typically within ±1 year per 10 counted years, see Figure 3 b)). Below 32.5 m WE, average annual layer thickness becomes close to 1 cm and counting in the CFA profile becomes increasingly difficult (i.e. frequent "shoulder type" annual layers merged into a single impurity peak). The LA-ICP-MS Ca profile continues to show distinct groups of peaks that become increasingly closely

15   spaced and eventually merge into single broad peak events (Figure 3 c)). Accordingly, LA-ICPMS Ca was the dominant source of annual layer counting after around 32.5 m WE (1600 AD). The annual layer signal remains clearly identifiable for the remaining part of the depth-range investigated here (e.g. apparently not affected by diffusion of soluble Ca).

4.3 Age constraints from radiocarbon analysis

For KCC, results from ^{14}C analysis are found to back the annual layer counted age scale. Five of six ^{14}C dates agree with

20   the counting within their 1-sigma range (Figure 4), corresponding to a root mean square deviation of 118 years (227 years including the outlier). The outlier ^{14}C point contradicts a monotonic increase of age with depth and is thus disregarded. This is justified, because the ^{14}C age of this sample matches with a very sensitive section of the ^{14}C-calibration curve. Therefore

already a small, unknown blank contribution would be able to shift the calibrated age of this sample significantly. Within the 2 sigma error range it also hits the error range of the annual layer counting chronology in the present configuration. Its deviation is therefore not of consequence.

For the KCI ice core, the radiocarbon ages are found to agree with the extension of the existing age scale based on the two-parameter model. It seems worth noting, however, that four out of five ^{14}C points lie systematically above the extrapolated age scale (albeit in agreement within their 1-sigma range). Only the sample at 28.4 m WE shows an age that is significantly older than expected. This can on one hand be due to the extremely small (also compared to the other KCI samples) sample size of only 2.2 μgC making this sample prone to even very small potential blank contributions. In this context also a potential influence of aged organic material (e.g. from Saharan dust) has to be regarded. At present, the age of this sample is therefore regarded as an outlier. Additional radiocarbon measurements of this core section above and below the critical sample are planned to further refine the match, and to test if the systematic deviation of the ^{14}C ages persists. The ^{14}C ages of the KCC and KCI samples are summarized in the appendix, Table A2.

4.4 Dating uncertainty

Potential sources of uncertainty in annual layer counting stem from i) erroneously identifying or missing of existing annual layers, ii) interpolating data gaps and iii) an incomplete stratigraphy missing years due to annual snowfall fully eroded from the surface. Regarding i), we estimated the likelihood of miscounting layers by marking "uncertain years" (Figure 3). In view of the high snow erosion at CG, uncertain layers were defined as additional peaks in close proximity to an annual layer (e.g. "shoulder type" peaks). To quantify counting uncertainty from uncertain layers, we followed the approach successfully employed for Greenland ice cores. This is to count uncertain layers as 0.5±0.5 years and to estimate the maximum counting error (MCE) from N uncertain layers as N x 0.5 years (Andersen et al., 2006; Rasmussen et al., 2006). With 144 uncertain layers detected within the upper 40 m WE of KCC, this corresponds to an uncertainty of ±72 years at 1000 AD. With respect to ii), the depth interval considered in this work was completely recovered without core loss. The ends of the CFA core sections were trimmed in case of irregular core breaks. This resulted typically in less than a centimeter of missing CFA data, thus not interfering with annual layer counting. The ECM profile was used as an alternative backup across these short CFA data gaps. Likewise, the CFA data was used as an alternative indicator where the LA-ICP-MS profile was incomplete, which only concerned one major instance of missing LA-ICP-MS data between about 33.8–34.24 m WE.

Contribution iii) constitutes a fundamental difference relative to Greenland conditions, since CG is not a closed system with respect to precipitation and loss of the annual snowfall in selected years can occur. The frequency of occurrence in these total snow loss events is, however, extremely hard to quantify. Counting annual layers in between the above mentioned (dust) horizons within the last century, reveals an offset of typically only one to two years as compared to the known age of the horizons. Thus, the counting appears not to be systematically flawed by missing years. Hence we regard uncertainty i) as dominant and use the MCE as an uncertainty estimation of the KCC age scale. Notably, the uncertainty refers to the unconstrained counting approach used here and could be further refined in the future with new absolute dating horizons, especially for the per-1900 AD period.
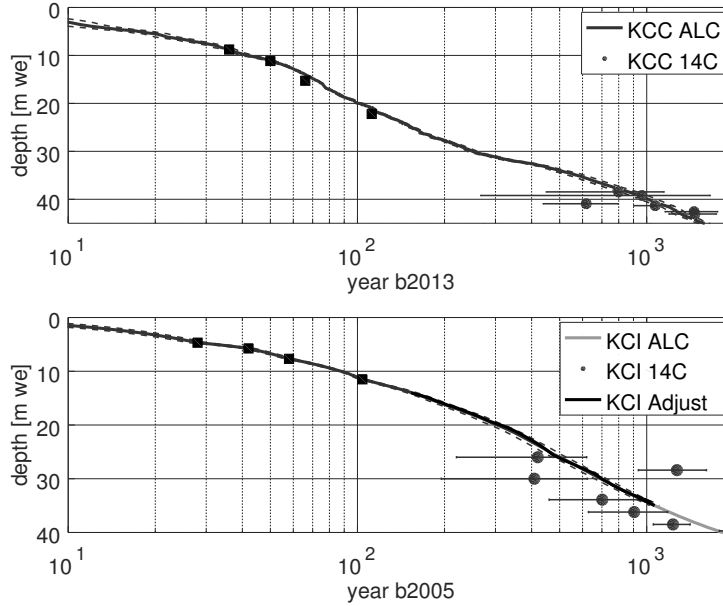
Figure 4. Age-depth relations over the last 1000 years for KCC and KCI, shown in the top and bottom row respectively. Age is plotted on a logarithmic axis, together with the according estimates of maximum dating uncertainty (dashed lines) and ^{14}C age constraints (with 1-sigma range) for KCC and KCI. Also shown is the adjusted age scale of KCI based on the stable water isotope time series comparison (solid black line, within less than 15 years of the original dating and thus hardly distinguishable here, see text). Absolute dating horizons used roughly within the last 100 years (see text) are shown as black squares. Note that the KCI chronology is based on a simple extrapolation below 26 m WE and has large uncertainty beyond the last 1000 years (thus indicated as light gray line only).

The uncertainty of the KCI age scale was obtained in a consistent manner, using the MCE for the annual layer counted interval and extrapolating the upper and lower uncertainty limits with the two-parametric model. Figure 4 shows the resulting age-depth relation and uncertainty bands for KCC and KCI, together with ^{14}C dates (shown with their 1–sigma uncertainty range) available for the respective depth interval. Table 3 gives a complementary summary of the age-depth relation, uncertainties and annual layer thickness for 10 m depth intervals. It is important to note that we are less confident about the age-depth relation of KCI compared to KCC, due to KCI featuring i) annual layering counting using only two bulk parameters and only down to 26 m WE and ii) the extrapolation by the two-parameter model.

4.5 Inter-core time series comparison and age scale alignment

To investigate potential offsets between the KCI chronology and the presumably more reliably dated KCC, we compared the stable water isotope time series of the two cores. This is motivated by the fact that the decadal isotope trends among the CG ice cores have been previously shown to agree over the last 250 years (Bohleber et al., 2013). Without substantial dating
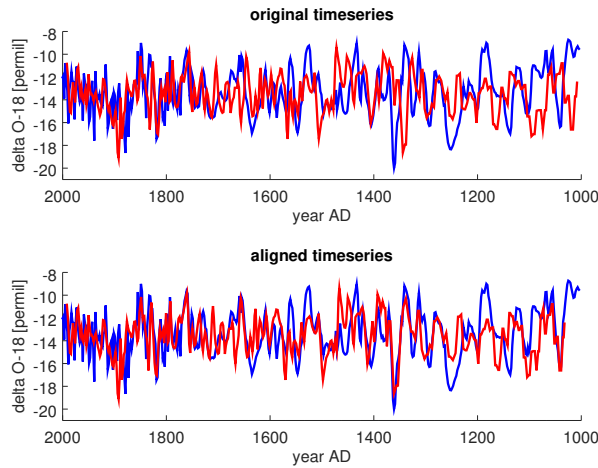
Figure 5. Stable water isotope time series of KCC and KCI, shown in blue and red, respectively. The top row shows both records on their original time scale over the last 1000 years. The KCI age scale was adjusted using the algorithm of (Lisiecki and Lisiecki, 2002) to optimise the match with KCC.

offset between the cores, this inter-core agreement should hold also on longer time intervals. It is important to note that due to the strong effect of isotope diffusion at CG, inter-annual or even seasonal isotope variability is effectively eliminated. As a consequence, the records (except for the last 100 years in KCC) resolve only decadal-scale variability at best. Hence we did not apply any further smoothing to the time series. In order to avoid potential biases from increasing sampling resolution, both
5   time series were sub-sampled to nominal biennial resolution. Figure 5 shows the comparison of the respective time series on their original time scales for the last 1000 years.

The two original time series of KCC and KCI already feature striking similarities, although frequently separated by a lag between the two time series (e.g. note the distinct isotope minima around 1360 AD). The direction and magnitude of this lag varies with time, hampering an absolutely straightforward adjustment to match the two records. Aiming to adjust the KCI
10   record to KCC time series, we employed the powerful algorithm developed by Lisiecki and Lisiecki (2002) for correlating paleoclimate time series. In doing so, we left the last 150 years of the KCI age scale unchanged (since considered reliably dated) but did not prescribe any further user-defined tie-points to the algorithm. The result shows the original lag between the two time series eliminated (Figure 5). A maximum shift of around 15 years is needed to align the two records (e.g. around the 1360 AD isotope minimum), which is within the estimated dating uncertainty of KCI (Figure 4). As a result, the aligned
15   time series are significantly correlated ($r = 0.47$). This degree of correlation is within the typical range of correlating CG isotope time series on the decadal scale within the last 250 years (Bohleber et al., 2013). However, this is the first time that the correlation holds to this extent also for the comparatively old core sections of CG ice cores, e.g. we find a correlation coefficient of $r = 0.50$ when considering the interval 1500–1000 AD only. In the following, all KCI time series are considered on their aligned time scale.

5 Results and Discussion

The age scale of KCC provides the first chronology of the last millennium for a CG ice core that is fully based on annual layer counting. The new KCC age scale offers the to-date most accurate foundation to study the CG proxy time series over long time scales, e.g. regarding the recent investigation pursuing the link with historical evidence by More et al. (2017) who used
5 a slightly adjusted version of the age scale presented here (albeit not significantly different with respect to uncertainty). The novel technique of LA-ICP-MS was crucial for a reliable identification of cm and sub-cm thin layers in the deeper parts of the core. Thereby, this work adds to recent studies (e.g. Della Lunga et al., 2017; Haines et al., 2016; Mayewski et al., 2014) to demonstrate the potential of the high-resolution impurity records afforded by LA-ICP-MS for investigating highly thinned sections of polar and alpine ice cores. The combination of high-resolution annual layer counting and radiocarbon analysis
10 promises a break-through also for dating highly thinned deep parts of ice cores drilled at other sites.

5.1 Stable water isotope records

The covariation of the $\delta^{18}O$ time series between KCI and KCC strongly suggests a common atmospheric driver, i.e. temperature. At first glance Figure 5 shows an increasing trend over the last 100 years but also generally higher mean isotope levels prior to about 1900 AD. This is in line with earlier findings suggesting an "early instrumental period" warmer than instru-
15 mental data by about $+0.4°C$ derived from the CG isotope signal (Bohleber et al., 2013). Here we find the generally higher average isotope levels to persist over much of the pre-industrial period: For instance, the mean $\delta^{18}O$ level in KCC between 1860-1000 AD is higher by about $0.75‰$ than the 2000-1860 AD average.. A quantitative use of the common isotope signal would therefore require addressing systematic so-called "upstream effects" and a reliable calibration of the isotope signal against instrumental temperature.
20 Upstream-effects concern the systematic variation in seasonality of the net accumulation upstream of the drilling site and have the potential to bias long-term core averages. Quantifying this effect requires accurate identification of the upstream catchment area (typically by sophisticated flow modeling) and evaluating the spatial variability in mean isotope levels. Dedicated efforts to evaluate the upstream-effect for the KCI-KCC flow line are currently underway (pers. comm. Carlo Licciulli and Josef Lier IUP Heidelberg). From a preliminary inspection of snow pit data recently obtained for the KCI-KCC flow line, there is no clear
25 indication of a systematic trend in mean $\delta^{18}O$ levels upstream of KCI, however: Comprising roughly the years 2016–2014, three snow pits evaluated thus far show mean $\delta^{18}O$ levels of -13.22, -11.94 and -15.04 ‰ at about 60, 195 and 300 m distance upstream of KCI, respectively (KCC is located roughly 110 m upstream of KCI, cf. Figure 1).
In order to calibrate the stable water isotope signal, we used the instrumental temperature dataset compiled in an earlier study (Bohleber et al., 2013). This temperature dataset (referred to here as "CG modified temperature") was specifically adjusted
30 to the CG ice core conditions, taking into account the summer bias in precipitation and snow deposition. To calculate an isotope/temperature sensitivity, we considered both KCC and KCI individually as well as a stack of the two stable isotope records (calculated as their simple average at nominal annual resolution). Using 2000–1860 AD as calibration period (thus deliberately avoiding the "early instrumental period" prior to 1860) our results reproduce earlier findings of Bohleber et al. (2013). This
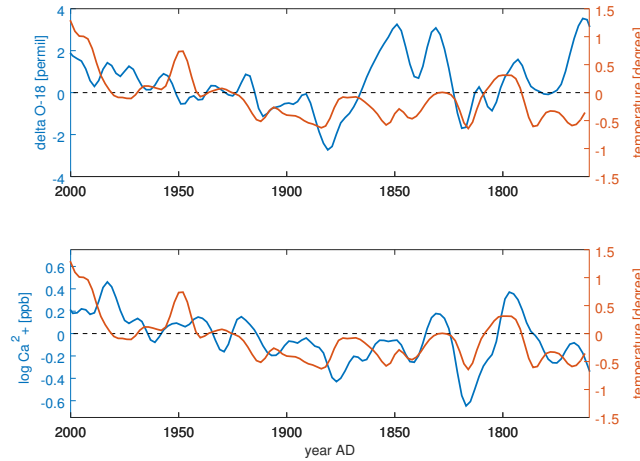
Figure 6. Comparison of KCC δ^{18}O and Ca^{2+} against the CG modified instrumental temperature (orange), shown in top and bottom, respectively, and covering the full instrumental period back to 1760 AD. Shown are anomalies relative to the respective 2000-1860 AD mean, and as decadal trends obtained from Gaussian smoothing.

specifically includes showing i) an overall agreement between the isotope and temperature record interrupted by characteristic decadal mismatch periods (Figure 6), ii) an increase in isotope/temperature correlation for multi-annual and decadal averages (e.g. $r = 0.33, 0.47, 0.64$ for discretely binned annual, 5 and 10 year averages, respectively in case of KCC) and iii) higher correlations obtained from the stack vs. the individual time series (e.g. $r = 0.48, 0.67, 0.79$ for annual, 5 and 10 year averages, respectively).

Regarding sensitivity values, we also find an increase with length in averaging period as well as substantially higher sensitivity values for KCI than KCC, revealing 2.3 vs. 1.4 ‰/°C, respectively, when using discretely binned 10-year averages (and 1.8 ‰/°C for the stacked record). Hence we obtain sensitivity values about threefold of what is expected, e.g. based on the isotope/temperature relationship of 0.65 ‰/°C reported by Rozanski et al. (1992) for European temporal trends in precipitation. Since a more strict confinement towards sampling the high summer season can be expected for the lower accumulation KCI, the sensitivity difference among KCI and KCC points towards the seasonal bias in snow samping to be connected with enhancing sensitivity. It is important to note that the high isotope-sensitivity deserves a separate thorough investigation, ideally comprising regional climate-isotope modeling and taking into account post-depositional effects such as snow preservation, upstream-effects and isotope diffusion, which is outside the scope of this study. Until an adequate long-term calibration of the CG isotope signal is achieved, however, we do not attempt a quantitative temperature reconstruction based on the isotope composite record so far.

Figure 7 shows the time series of δ^{18}O in comparison with Ca^{2+}, deuterium excess and CPP. Due to the logarithmic distribution of the Ca^{2+} data, we generally use a log-scale to show the Ca^{2+} time series. For KCC, we find δ^{18}O and Ca^{2+} to be significantly correlated over the last 1000 years (at $r = 0.49$, cf. Figure 7). This suggests that the common decadal-scale
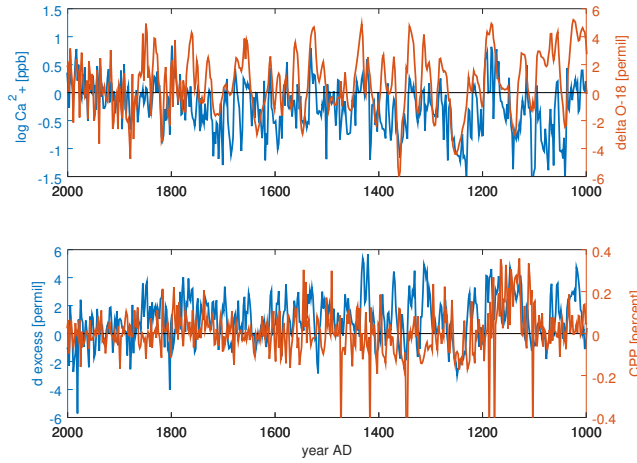
Figure 7. Records of KCC, displaying $\delta^{18}O$ together with Ca^{2+} (top row) and deuterium excess together with the coarse particle percentage (CPP, bottom row), shown in blue and orange, respectively. All time series are shown as anomalies relative to the respective 2000–1860 AD mean at biennial resolution. Note the high levels of deuterium excess and CPP around 1100–1200 AD.

signal driver behind the shared variability between the $\delta^{18}O$ time series of KCC and KCI also holds for Ca^{2+}. Prior to about 1860 AD, the $\delta^{18}O$ time series constitutes nearly an upper envelope signal as compared to Ca^{2+}. Short excursions to low Ca^{2+} concentrations missing a respective counterpart in $\delta^{18}O$ may have been smoothed out by isotope diffusion. Worth noting in this respect, the firn-ice transition in KCC coincides roughly with the last 100 years in the record (Tables 1 and 3).

5.2 Mineral dust proxy records

Following our general distinction (section 2), two signal components of the Ca^{2+} time series are investigated separately: i) the frequency of occurrence in Saharan dust deposition, and ii) the long-term average Ca^{2+} concentration. In order to investigate to what extent the time series agreement observed for $\delta^{18}O$ also holds in case of mineral dust related species, we use the insoluble particle signal as a surrogate for Ca^{2+} (since Ca^{2+} has not been measured for KCI). Figure 8 shows an overview of the insoluble particle datasets of KCC and KCI. KCC data shows that the insoluble particle signal and Ca^{2+} concentrations are generally highly correlated (e.g. $r = 0.9$ within the last 1000 years). The KCC-KCI inter-core comparison of insoluble particle records reveals agreement of decadal scale features, as well as similarities regarding periods of low concentrations and higher peak abundance (e.g. 1800–1820 vs. 1780–1800, respectively). Differences in the magnitude of individual peak events as well as mean levels of particle concentrations can be explained in light of i) the KCI particle signal measured on diluted sample meltwater, ii) potential calibration differences in the optical particle sensor and iii) inter-site snow deposition variability. Accordingly, it was not attempted to construct a composite record of insoluble particles from the two cores.
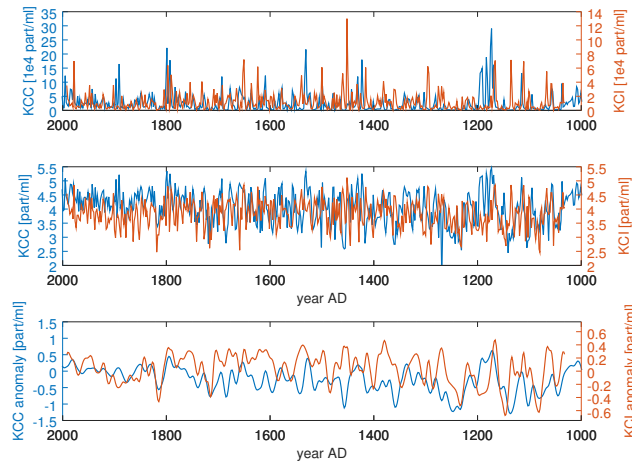
Figure 8. Inter-core comparison of the insoluble particle signal of KCC (blue) and KCI (orange). The top and middle row show the insoluble particle time series on a linear and logarithmic scale, respectively. The bottom row shows decadal trends of anomalies with respect to their 2000–1860 AD mean, highlighted by Gaussian smoothing. The KCI record is on the adjusted time scale after matching the stable water isotope records.

5.2.1 Detection of Saharan dust peak events and frequency of occurrence

Essential for the calculation of a robust occurrence rate of dust events are adequate means to distinguish desert dust from background and from deposition events of long-range transported anthropogenic pollutants. While the particle signal alone is not sufficient for differentiating these events, Saharan dust layers in CG ice cores can be reliably identified based on the
5   analyses of Ca^{2+}, supplemented by alkalinity measurements and, in principle, particle size distribution (Wagenbach et al., 1996). The central criteria used in this study in order to identify Saharan dust are strongly elevated concentrations of Ca^{2+} coinciding with acidity values reduced to alkaline levels. Since no direct acidity measurements are available in our case from CFA, we rely on the ECM record for this purpose. At CG high dust levels are able to reduce the ECM signal to almost zero (rendering the ECM to be a qualitative dust indicator rather than an quantitative acidity gauge). Dust anomalies were identified
10   as "peaks over threshold". A robust spline smoothing was used to remove the general trend from the Ca^{2+}-data. Peak events then needed to exceed three times the median absolute deviations (Figure 9). We have also used the particle size distribution to investigate exemplarily a small number of dust events, finding that dust events show systematically higher CPP with respect to dust-free core sections.

To detect the frequency of occurrence in dust peak events, we followed the statistical tool outlined in Chapter 6 of Mudelsee
15   (2010). For a non-parametric occurrence rate estimate we used a moving Gaussian kernel (bandwidth 51 years) and accounted for boundary effects. For KCC, only the subset of peak events coinciding with a vanishing ECM signal was considered to be of Saharan dust origin. For KCI, we employed the same peak detection scheme to the insoluble particle signal. However, due
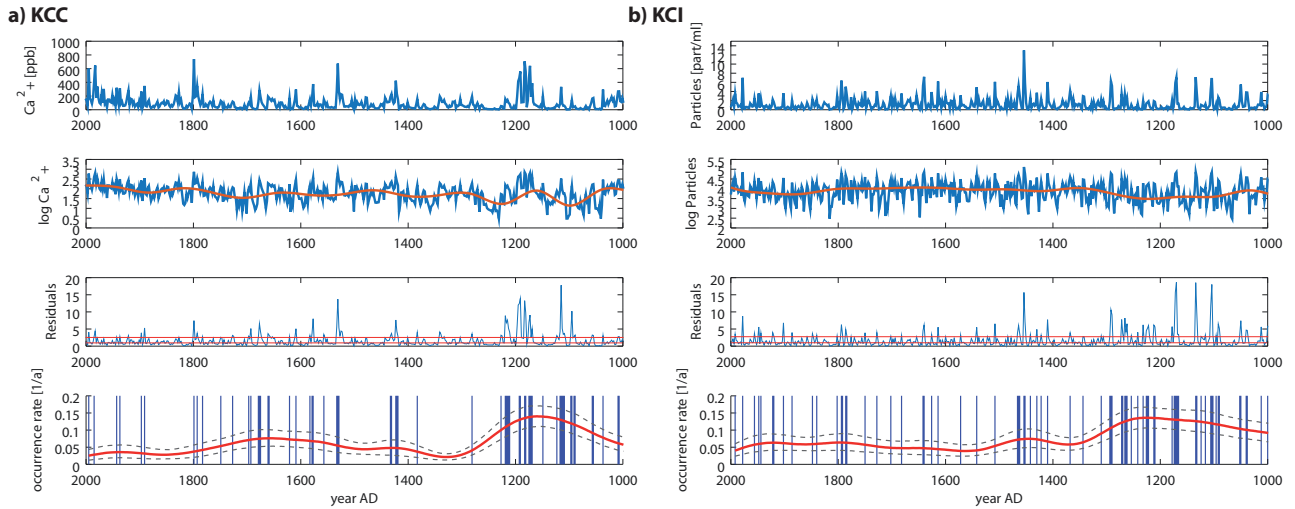
Figure 9. Results from detecting Saharan dust events in the ice core records and estimating their long-term frequency of occurrence. Figure part a) corresponds to KCC, part b) to KCI (see text). The bottom row shows the detected events (blue) and the frequency of occurrence kernel estimate with a 51-year bandwidth (bottom rows, in red) together with 90% confidence intervals.

to the lack of a full ECM profile, no subset corresponding to low acidity could be defined. Using a direct comparison with the insoluble particle signal of KCC, with and without ECM correction, we found that the respective uncorrected frequency of occurrence is expected to contain a minor bias towards higher peak abundances, but leaves the overall features unchanged. As the main robust features for KCC and KCI, the frequency of occurrence in dust peaks is systematically increased prior to 1250 AD with respect to the rest of the record (Figure 9). Dust anomalies are found clustered in periods around 1100–1200 (extending into the 1200s), around 1400–1450 and, for KCC only, between 1500–1800. This is in broad agreement with enhanced Saharan dust deposition reported by Thevenon et al. (2009) for periods around 1200–1300, 1430–1520, 1570–1690, 1780–1800, and after 1870. The latter periods were identified by Thevenon et al. (2009) based on sophisticated elemental analysis in a CG ice core, albeit at much coarser resolution and larger dating uncertainty, which hampers a more detailed comparison. However, in our data we also recognize a large dust peak located between 1780 and 1800 which was suggested as a dating reference horizon by Thevenon et al. (2009).

5.2.2 The long-term Ca^{2+} variability in relation to temperature

Within the calibration period 2000–1860 AD, we find the overall increasing trend in instrumental temperature to be represented also in increasing levels of $\delta^{18}O$ and Ca^{2+} (Figure 6). The Ca^{2+} signal correlates significantly with the CG modified instrumental temperature at $r = 0.41, 0.56, 0.71$ using biennial, 5 and 10 year averages, respectively, within the calibration period. Nearly identical correlation values are obtained for the full instrumental period back to 1760 AD. Within the calibration period (Figure 6), we compared the decadal trends (highlighted by Gaussian smoothing) of the CG modified instrumental tempera-

ture with $\delta^{18}O$ and Ca^{2+}, respectively. The comparison reveals that the Ca^{2+} signal performs similarly to $\delta^{18}O$ in explaining variance of the temperature data (both at around 25%, although only interpreted with caution due to the autocorrelation of the smoothed curves).

Potential drivers for a Ca^{2+}-temperature coupling can be expected from i) the advection of air masses comprising a high Saharan dust load generally being associated with warm temperatures (Wagenbach et al., 1996), ii) the deposition of dust leading to lowered snow albedo thus supporting surface snow consolidation (Haeberli et al., 1983) and iii) warm temperature favoring snow consolidation (e.g. Fauve et al., 2002; Haeberli et al., 1983). However, it generally remains difficult to quantify the influence of the above processes. It seems worth pointing out that, process iii) acts independently from the type of impurity / isotope species considered. Likewise, a similar process as i) may be envisaged in case of $\delta^{18}O$. However, process ii) mainly concerns dust-related species such as Ca^{2+} providing an essential "self-preserving" character for these species with respect to snow deposition. Regarding this connection between dust content and presumed faster snow preservation, supporting evidence is provided by including the high-resolution density profile of KCC. Comparing profiles of Ca^{2+} and density reveals that layers with a high dust load generally coincide with layers of enhanced density (Figure A2 in the appendix). Regarding process iii), we made an attempt to semi-quantitatively explore the imprint of snow preservation on the long-term variability in Ca^{2+} (appendix A1). Previous studies already used simplified conceptual models to investigate the influence of snow deposition on seasonal ice core signals, and demonstrated the decisive role played by the amplitude of the seasonality (Wagenbach et al., 2012; Fisher and Koerner, 1988). We employed the model by Wagenbach et al. (2012), with parameters reflecting to CG snow preservation conditions. This revealed that the resulting bias from incomplete snow preservation on the average Ca^{2+} level is already in the same order of magnitude as the long-term Ca^{2+} trends found in previous studies (Wagenbach et al., 1996) and also in the core investigated here. As a result, the influence of snow deposition appears non-negligible in explaining the apparent Ca^{2+}-temperature co-variation. Notably this implies that, at best, the Ca^{2+}-temperature coupling allows for using Ca^{2+} trends as a site-specific temperature proxy only. This is in analogue to the study by Kellerhals et al. (2010a) demonstrating temperature-related variability for NH_4^+ at a low-latitude site, albeit explained by a different mechanism than discussed for Ca^{2+} at CG here.

5.3 Temperature and mineral dust variability over the last millennium

Based on the above considerations and the agreement within the instrumental period (Figure 6), the potential of the Ca^{2+} signal to quantitatively record temperature variability is explored further over the full 1000 year period. For this purpose the biennial logarithmic Ca^{2+} is calibrated tentatively against instrumental temperature using linear regression within the time period 2006–1860 AD. The respective 90% confidence intervals are used to calculate a temperature reconstruction with uncertainty bands (0.7–1–1.8 $°C$/log Ca^{2+} [ppb]). Decadal trends are again highlighted by Gaussian smoothing in Figure 10. The resulting 1000-year record is shown with a tentative 200-year extension. Regarding its overall features and in view of remaining dating uncertainties, the record provides evidence of "Little Ice Age conditions" systematically cooler than the reference and calibration period, with an average of $-0.3°C$ between 1800–1200 AD. A shorter warm interval of about $+0.3°C$ is found in the late 1100s These features are especially noteworthy considering the above-average mean of the $\delta^{18}O$ values with respect
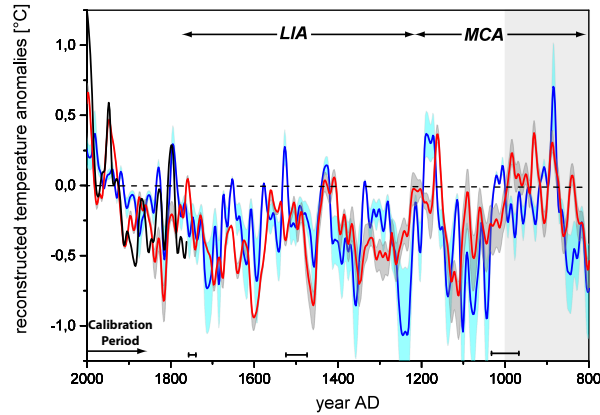
Figure 10. Comparison of decadal temperature trends as anomalies with respect to the mean of 2006–1860 AD. Shown are calibrated temperatures obtained from the KCC Ca^{2+} variability (blue lines, with uncertainty indicated as light blue bands). Also shown are instrumental temperature data (black) and the summer temperature reconstruction of Luterbacher et al. (2016) in red (uncertainty as gray bands). Note that the overall co-variation among the two reconstructions persists for at least another 200 years beyond 1000 AD (light gray shaded area). Black bars on the bottom indicate maximum dating uncertainty.

to 2006–1860 AD (Figure 7). The comparison with $\delta^{18}O$ suggests that the Ca^{2+}-temperature coupling may be less affected by non-stationary sensitivity (and upstream) effects.

In this context we further explored our Ca^{2+}-based temperature-reconstruction attempt in comparison with other proxy reconstructions of European summer temperature. We show here results from using the mean European summer temperature

5   anomalies reconstructed by Luterbacher et al. (2016), considering their composite-plus-scaling method (CPS) adjusted to biennial resolution and our reference time period of 2006–1860 AD. The decadal trends (represented by Gaussian smoothing) of both reconstructions shown in Figure 10 are generally consistent in their overall features (and formally correlate at $r = 0.4$). These features comprise the recent warming trend and below average conditions during the "Little Ice Age" (LIA), and a warm episode in the late 1100s ("Medieval Climate Anomaly", MCA). The only major feature of disagreement occurs around the

10   already noted minimum around 1250–1230 AD. The overall low levels of impurities (especially NH_4^+) and $\delta^{18}O$ may point to increased deposition of winter snow during this time, or exceptionally cold summer conditions. It is worth noting that if, tentatively, extending the comparison for another 200 years beyond 1000 AD, the agreement between the two reconstructions continues to last until 800 AD, consistently showing a relatively warm interval lasting between about 1000–850 AD. The overall agreement is especially noteworthy in the light of: i) Only small offsets exist between the general features of the two

15   records, which may stem from the remaining dating uncertainty of KCC. The comparison is not intended as a dating validation, however. ii) The absence of evidence of a non-stationary sensitivity. The magnitude of the general features (LIA, MCA) and decadal scale temperature variability derived from our ice core record is consistent overall with the other proxy reconstruction. A potential systematic bias to the observed Ca^{2+}-temperature coupling could arise from strong and long-term changes at the

dust source, e.g. increased dust mobilization, which could also affect the long-term Ca^{2+} variability. At the same time, increased dust mobilization would likely also influence the Saharan dust spikes and their frequency of occurrence. However, we only find one instance of long-term changes in dust occurrence rate. Being the most outstanding period in the dust event occurrence warrants taking a closer look at 1100–1200 AD. This outstanding period is characterized by i) an increased frequency of Saharan dust events, ii) its above average levels, both in CPP and deuterium excess, starting to rise around 1100 AD, and iii) a delayed relative increase in $\delta^{18}O$ and Ca^{2+}, e.g. first showing minimum concentrations between 1130–1170 AD followed by a shorter maxima around 1170–1200 AD. The CPP maximum constitutes the dominant feature of the entire record (notably, this result does not depend of the exact threshold chosen to calculate the CPP). The median of the CPP record within this 1100–1200 AD time period (0.61 ± 0.11, reported with one median absolute deviation) indicates an increase in coarse particles by about 12% relative to the median of the rest of the 1000-year time period (0.48 ± 0.05). While an increase in dust mobilization cannot be ruled out, the connection of the distinct increase in coarse particles with enhanced dust event frequency rather suggests an increase in the direct transport of Saharan dust (as opposed to indirect advection with longer pathway and thus stronger decrease in coarse particles). Finding increased values of deuterium excess supports the view of a relative increase in direct Saharan dust advection, as increased deuterium excess could be expected from warm and dry air masses collecting moisture over the Mediterranean (e.g. Pfahl and Sodemann, 2014). Overall these findings motivate getting an even more detailed picture of this outstanding period, e.g. using isotopic fingerprinting of the dust layers for a precise provenance investigation, which is left for future investigations..

6   Conclusions and Outlook

A combination of state-of-the-art methods in ice core analysis allowed us to date the latest CG ice core KCC with unprecedented confidence. The breakthrough in this respect was to extend annual layer counting, for the first time at CG, over more than the last 1000 years and finding the resulting age scale corroborated by radiocarbon analyses. The combination of high-resolution annual layer counting afforded by LA-ICP-MS with constraints from radiocarbon analyses could be employed with great success also at deep sections of other (mountain) ice cores. By means of the improved age scale it became possible, for the first time, to demonstrate that the inter-core agreement in decadal isotope variability among two cores on the same flow line extends over the last 1000 years. The inter-core agreement suggests a common driver of the shared signal, also extending to the long-term variability in Ca^{2+}. We find substantial agreement among the decadal trends of Ca^{2+} and temperature at CG, over the entire instrumental period. Since snow preservation plays a key role for the observed coupling between Ca^{2+} and instrumental temperature, this makes Ca^{2+} trends at best a site-specific temperature proxy, although it remains to be tested to what degree the association with temperature also holds at other alpine drilling sites. In contrast to the stable isotope signal at CG, however, we find no evidence of non-stationary temperature sensitivity for Ca^{2+}: Exploiting the Ca^{2+}-temperature agreement for a quantitative reconstruction i) proves to be consistent with other latest summer temperature reconstructions, and ii) reproduces overall features regarding the "Little Ice Age" and the "Medieval Climate Anomaly". Parameters less influenced by snow preservation (dust event occurrence rate and particle size distribution) reveal an exceptional medieval period around 1100–

1200 AD, suggesting a relative increase in meridional flow and dry conditions over the Mediterranean during that time. Future and ongoing investigations will target the application of our new dating approach to the bottom 10 m WE of KCC, and an improved quantitative understanding of the isotope-thermometer at CG. In this context a central question remains whether the isotope-based temperature signal can be reconciled quantitatively with the Ca^{2+}-based reconstruction.

5   *Acknowledgements.*   We are grateful to numerous colleagues for their commitment regarding field work, ice core drilling and ice core analyses. In particular we would like to acknowledge the support of the Initiative for the Science of the Human Past at Harvard University and all its project members. Additional invaluable support in ice core processing was provided by the Alfred-Wegener-Institute, Helmholtz Center for Polar and Marine Research, Bremerhaven (AWI). The Klaus-Tschira-Lab Mannheim is acknowledged for their support in radiocarbon analysis. We also would like to thank Johanna Kerch, Carlo Licciulli, Josef Lier and Lars Zipf from IUP Heidelberg for their support. We

10   thank Johannes Freitag (AWI Bremerhaven) for the high-resolution density data. Recovery and analysis of the 2013 CG ice core KCC were supported by the Arcadia Fund of London (AC3450) and the Helmholtz Climate Initiative REKLIM. Work on the 2005 CG ice core KCI has been funded by the European Union under contract ENV4-CT97-0639 (project ALPCLIM) and within the project ALP-IMP through grant EVK2-CT2002-00148. LA-ICP-MS ice core analyses were conducted in the Climate Change Institute's W. M. Keck Laser Ice Facility at the University of Maine supported from the W. M. Keck Foundation and the National Science Foundation (PLR-1042883, PLR-1203640).

15   Financial support was provided to P.B. by the Deutsche Forschungsgemeinschaft (BO 4246/1-1). We would like to especially thank and acknowledge our late colleague Dietmar Wagenbach (Heidelberg University) for his long-standing contributions to glaciological research at Colle Gnifetti, and in particular for sharing his unique expertise with us at the early stage of our project.

References

Ahmed, M., Anchukaitis, K. J., Asrat, A., Borgaonkar, H. P., Braida, M., Buckley, B. M., Büntgen, U., Chase, B. M., Christie, D. A., Cook, E. R., et al.: Continental-scale temperature variability during the past two millennia, Nature Geoscience, 6, 339, 2013.

Alean, J., Haeberli, W., and Schädler, B.: Snow accumulation, firn temperature and solar radiation in the area of the Colle Gnifetti core drilling site (Monte Rosa, Swiss Alps): distribution patterns and interrelationships, Zeitschrift für Gletscherkunde und Glazialgeologie, 19, 131–147, 1983.

Andersen, K. K., Svensson, A., Johnsen, S. J., Rasmussen, S. O., Bigler, M., Röthlisberger, R., Ruth, U., Siggaard-Andersen, M.-L., Steffensen, J. P., Dahl-Jensen, D., et al.: The Greenland ice core chronology 2005, 15–42ka. Part 1: Constructing the time scale, Quaternary Science Reviews, 25, 3246–3257, 2006.

Bohleber, P., Wagenbach, D., Schöner, W., and Böhm, R.: To what extent do water isotope records from low accumulation Alpine ice cores reproduce instrumental temperature series?, Tellus B, 65, 2013.

Brook, E. J., Wolff, E., Dahl-Jensen, D., Fischer, H., Steig, E. J., et al.: The future of ice coring: international partnerships in ice core sciences (IPICS), PAGES news, 14, 6–10, 2006.

Della Lunga, D., Müller, W., Rasmussen, S. O., Svensson, A., and Vallelonga, P.: Calibrated cryo-cell UV-LA-ICPMS elemental concentrations from the NGRIP ice core reveal abrupt, sub-annual variability in dust across the GI-21.2 interstadial period, The Cryosphere, 11, 1297–1309, doi:10.5194/tc-11-1297-2017, http://www.the-cryosphere.net/11/1297/2017/, 2017.

Fauve, M., Rhyner, H., and Schneebeli, M.: Pistenpräparation und Pistenpflege: ein Handbuch für den Praktiker, Eidgen. Inst. für Schnee-u. Lawinenforschung, 2002.

Fisher, D. A. and Koerner, R. M.: The effects of wind on $\delta(^{18}O)$ and accumulation give an inferred record of seasonal δ amplitude from the Agassiz ice cap, Ellesmere Island, Canada, Annals of Glaciology, 10, 34–37, 1988.

Gabrielli, P., Barbante, C., Bertagna, G., Bertó, M., Binder, D., Carton, A., Carturan, L., Cazorzi, F., Cozzi, G., Dalla Fontana, G., et al.: Age of the Mt. Ortles ice cores, the Tyrolean Iceman and glaciation of the highest summit of South Tyrol since the Northern Hemisphere Climatic Optimum, The Cryosphere, 10, 2779, 2016.

Haeberli, W. and Funk, M.: Borehole temperatures at the Colle Gnifetti core-drilling site (MonteRosa, Swiss Alps), Journal of Glaciology, 37, 37–46, 1991.

Haeberli, W., Schotterer, U., Wagenbach, D., Schwitter, H. H., and Bortenschlager, S.: Accumulation characteristics on a cold, high-Alpine firn saddle from a snow-pit study on Colle Gnifetti, Monte Rosa, Swiss Alps, Journal of Glaciology, 29, 260–271, 1983.

Haeberli, W., Schmid, W., and Wagenbach, D.: On the geometry, flow and age of firn and ice at the Colle Gnifetti core drilling site (Monte Rosa, Swiss Alps), Zeitschrift für Gletscherkunde und Glazialgeologie, 24, 1–19, 1988.

Haines, S. A., Mayewski, P. A., Kurbatov, A. V., Maasch, K. A., Sneed, S. B., Spaulding, N. E., Dixon, D. A., and Bohleber, P. D.: Ultra-high resolution snapshots of three multi-decadal periods in an Antarctic ice core, Journal of Glaciology, 62, 31–36, 2016.

Hoelzle, M., Darms, G., Lüthi, M. P., and Suter, S.: Evidence of accelerated englacial warming in the Monte Rosa area, Switzerland/Italy, The Cryosphere, 5, 231–243, 2011.

Hoffmann, H., Friedrich, R., Kromer, B., and Fahrni, S.: Status report: Implementation of gas measurements at the MAMS 14C AMS facility in Mannheim, Germany, Nuclear Instruments and Methods in Physics Research Section B: Beam Interactions with Materials and Atoms, 410, 184 – 187, doi:https://doi.org/10.1016/j.nimb.2017.08.018, 2017a.

Hoffmann, H., Preunkert, S., Legrand, M., Leinfelder, D., Bohleber, P., Friedrich, R., and Wagenbach, D.: A new sample preparation system for micro-14C dating of glacier ice with a first application to a high Alpine ice core from Colle Gnifetti (Switzerland), Radiocarbon, in press, 2017b.

Hoffmann, H. M.: Micro radiocarbon dating of the particulate organic carbon fraction in Alpine glacier ice: method refinement, critical evaluation and dating applications, Ph.D. thesis, Heidelberg University, http://www.ub.uni-heidelberg.de/archiv/20712, 2016.

Jenk, T. M., Szidat, S., Bolius, D., Sigl, M., Gäggeler, H. W., and co-authors: A novel radiocarbon dating technique applied to an ice core from the Alps indicating late Pleistocene ages, Journal of Geophysical Research, 114, D14 305, 2009.

Kellerhals, T., Brütsch, S., Sigl, M., Knüsel, S., Gäggeler, H. W., and Schwikowski, M.: Ammonium concentration in ice cores: A new proxy for regional temperature reconstruction?, Journal of Geophysical Research: Atmospheres, 115, 2010a.

Kellerhals, T., Tobler, L., Brütsch, S., Sigl, M., Wacker, L., Gäggeler, H. W., and Schwikowski, M.: Thallium as a tracer for preindustrial volcanic eruptions in an ice core record from Illimani, Bolivia, Environmental Science & Technology, 44, 888–893, 2010b.

Konrad, H., Bohleber, P., Wagenbach, D., Vincent, C., and Eisen, O.: Determining the age distribution of Colle Gnifetti, Monte Rosa, Swiss Alps, by combining ice cores, ground-penetrating radar and a simple flow model, Journal of Glaciology, 59, 179–189, 2013.

Lisiecki, L. E. and Lisiecki, P. A.: Application of dynamic programming to the correlation of paleoclimate records, Paleoceanography, 17, 2002.

Luterbacher, J., Werner, J., Smerdon, J. E., Fernández-Donado, L., González-Rouco, F., Barriopedro, D., Ljungqvist, F. C., Büntgen, U., Zorita, E., Wagner, S., et al.: European summer temperatures since Roman times, Environmental Research Letters, 11, 024 001, 2016.

Lüthi, M. P. and Funk, M.: Dating ice cores from a high Alpine glacier with a flow model for cold firn, Annals of Glaciology, 31, 69–79, 2000.

Mayewski, P. A., Sneed, S. B., Birkel, S. D., Kurbatov, A. V., and Maasch, K. A.: Holocene warming marked by abrupt onset of longer summers and reduced storm frequency around Greenland, Journal of Quaternary Science, 29, 99–104, doi:10.1002/jqs.2684, http://doi.wiley.com/10.1002/jqs.2684, 2014.

More, A. F., Spaulding, N. E., Bohleber, P., Handley, M. J., Hoffmann, H., Korotkikh, E. V., Kurbatov, A. V., Loveluck, C. P., Sneed, S. B., McCormick, M., and Mayewski, P. A.: Next generation ice core technology reveals true minimum natural levels of lead (Pb) in the atmosphere: insights from the Black Death, GeoHealth, pp. n/a–n/a, doi:10.1002/2017GH000064, http://dx.doi.org/10.1002/2017GH000064, 2017GH000064, 2017.

Mudelsee, M.: Climate Time Series Analysis, Springer, 2010.

Nye, J.: Correction factor for accumulation measured by the thickness of the annual layers in an ice sheet, Journal of Glaciology, 4, 785–788, 1963.

Pfahl, S. and Sodemann, H.: What controls deuterium excess in global precipitation?, Climate of the Past, 10, 771, 2014.

Preunkert, S. and Wagenbach, D.: An automatic recorder for air/firn transfer studies of chemical aerosol species at remote glacier sites, Atmospheric Environment, 32, 4021–4030, 1998.

Preunkert, S., Wagenbach, D., Legrand, L., and Vincent, C.: Col du Dôme (Mt Blanc Massif, French Alps) suitability for ice-core studies in relation with past atmospheric chemistry over Europe, Tellus, 52B, 993–1012, 2000.

Prodi, F. and Fea, G.: A case of transport and deposition of Saharan dust over the Italian peninsula and southern Europe, Journal of Geophysical Research: Oceans (1978–2012), 84, 6951–6960, 1979.

Ramsey, B.: C. OxCal Program v4. 2.4, Radiocarbon Accelerator Unit, Univ. Oxford, 2016.

Rasmussen, S. O., Andersen, K. K., Svensson, A., Steffensen, J. P., Vinther, B. M., Clausen, H. B., Siggaard-Andersen, M.-L., Johnsen, S. J., Larsen, L. B., Dahl-Jensen, D., et al.: A new Greenland ice core chronology for the last glacial termination, Journal of Geophysical Research: Atmospheres, 111, 2006.

Rozanski, K., Araguas-Araguas, L., and Gonfiantini, R.: Relation Between Long-Term Trends of Oxygen-18 Isotope Composition of Precipitation and Climate, Science, 258, 981–985, 1992.

Ruth, U., Wagenbach, D., Steffensen, J. P., and Bigler, M.: Continuous record of microparticle concentration and size distribution in the central Greenland NGRIP ice core during the last glacial period, Journal of Geophysical Research: Atmospheres, 108, 2003.

Schwerzmann, A., Funk, M., Blatter, H., Lüthi, M., Schwikowski, M., and Palmer, A.: A method to reconstruct past accumulation rates in alpine firn regions: A study on Fiescherhorn, Swiss Alps, Journal of Geophysical Research: Earth Surface, 111, 2006.

Schwikowski, M., Seibert, P., Baltensperger, U., and Gaggeler, H.: A study of an outstanding Saharan dust event at the high-alpine site Jungfraujoch, Switzerland, Atmospheric Environment, 29, 1829–1842, 1995.

Sneed, S. B., Mayewski, P. A., Sayre, W. G., Handley, M. J., Kurbatov, A. V., Taylor, K. C., Bohleber, P., Wagenbach, D., Erhardt, T., and Spaulding, N. E.: New LA-ICP-MS cryocell and calibration technique for sub-millimeter analysis of ice cores, Journal of Glaciology, 61, 233, 2015.

Sodemann, H., Palmer, A., Schwierz, C., Schwikowski, M., and Wernli, H.: The transport history of two Saharan dust events archived in an Alpine ice core, Atmospheric Chemistry and Physics Discussions, 5, 7497–7545, 2005.

Stuiver, M. and Polach, H.: Discussion: Reporting of 14C data., Radiocarbon, 19, 355–63., 1977.

Thevenon, F., Anselmetti, F. S., Bernasconi, S. M., and Schwikowski, M.: Mineral dust and elemental black carbon records from an Alpine ice core (Colle Gnifetti glacier) over the last millennium, Journal of Geophysical Research: Atmospheres, 114, 2009.

Uglietti, C., Zapf, A., Jenk, T. M., Sigl, M., Szidat, S., Salazar Quintero, G. A., and Schwikowski, M.: Radiocarbon dating of glacier ice: overview, optimisation, validation and potential, The Cryosphere, 10, 3091–3105, 2016.

Wagenbach, D.: Environmental Records in Alpine Glaciers, in: The Environmental Record in Glaciers and Ice Sheets, edited by Oeschger, H. and C. C. Langway, Jr., pp. 69–83, John Wiley and Sons, 1989.

Wagenbach, D.: Special problems of mid-latitude glacier ice-core research. In: Greenhouse Gases, Isotopes and Trace Elements in Glaciers as Climatic Evidence of the Holocene, vol. Arbeitsheft Nr.14 of *Report of the ESF/EPC Workshop, Zürich 27-28 October 1992*, Versuchsanstalt für Wasserbau, Hydrologie und Glaziologie der Eidgenössischen Technischen Hochschule Zürich, 1992.

Wagenbach, D. and Geis, K.: The mineral dust record in a high altitude glacier (Colle Gnifetti, Swiss Alps), in: Paleoclimatology and Paleometeorology: Modern and Past Patterns of Global Atmospheric transport, edited by M, L. and M, S., pp. 543–564, Kluwer Academic Publishers, Dordrecht, 1989.

Wagenbach, D., Preunkert, S., Schäfer, J., Jung, W., and Tomadin, L.: Northward transport of Saharan dust recorded in a deep Alpine ice core, in: The impact of desert dust across the Mediterranean, pp. 291–300, Springer, 1996.

Wagenbach, D., Bohleber, P., and Preunkert, S.: Cold alpine ice bodies revisited: What may we learn from their isotope and impurity content?, Geografiska Annaler: Series A, Physical Geography, 94, 245–263, 2012.

Appendix A: Supplementary Material

A1 A semi-quantitative treatment of the snow deposition influence on average Ca^{2+}-concentrations and a possible coupling to atmospheric temperature

We attempt to semi-quantitatively explore the imprint of snow preservation on the long-term variability in Ca^{2+}, using the conceptual model by Wagenbach et al. (2012) and considering $\delta^{18}O$ as a reference. The model assumes sinusoidal cycles for the precipitation-borne signal $S(t)$ and the surface accumulation pattern $A(t)$, and a phase-lag t_ϕ between $S(t)$ and $A(t)$. The deviation Δ of the mean signal recorded in the firn at CG ($\bar{S}_{\mathrm{firn}}$) with respect to the overall mean signal (S_0) in the precipitation then becomes (corresponding to equation (5) in Wagenbach et al. (2012)):

$$S(t) = S_0(1 + s_r\,sin\,\omega(t + t_\phi)) \qquad A(t) = A_0(1 + a_r\,sin\,\omega t) \qquad \Delta = \bar{S}_{\mathrm{firn}} - S_0 = S_0\,s_r\,a_r\,cos\,\omega t_\phi \qquad \text{(A1)}$$

with a_r and s_r denoting the relative signal amplitudes, t_ϕ the temporal phase shift between the two cycles and ω the cycle frequency equal to $2\pi/T$ (period T = 1 yr). We reproduced here the calculation for $\delta^{18}O$ by Wagenbach et al. (2012) with typical seasonality parameters at Colle Gnifetti (e.g. $a_r = 0.8$). To estimate Δ for Ca^{2+}, we used values reported by Preunkert et al. (2000) for CG, i.e. taking $S_0 = 112$ ppb (the average of typical summer and winter concentrations) as well as $s_r = 0.64 \pm 0.26$. Notably, this value of s_r for Ca^{2+} is close to the absolute value of $s_r = 0.5$ obtained for $\delta^{18}O$ by Wagenbach et al. (2012). Estimating the radiation-induced control of snow consolidation on the seasonal net accumulation cycle at CG is consistent with a phase shift of $t_\phi = 1.5$ months (broadly equal to the delay of the isotope/aerosol peak with respect to insolation (Wagenbach et al., 2012)). Figure A3 shows the deviation Δ for Ca^{2+} and $\delta^{18}O$ as a function of phase shift t_ϕ and a_r.

The framework of the conceptual model allows us to semi-quantitatively explore a potential coupling of the long-term Ca^{2+} signal to atmospheric temperature via snow preservation effects. For instance, the effect of warmer atmospheric summer temperatures on snow preservation is envisaged as increased summer snow deposition, corresponding to an according change in a_r and, an additional possibility, a change in phase-shift t_ϕ. In the model, a more efficient snow-preservation for dust-rich layers would correspond to a decrease in phase-shift t_ϕ. We follow Wagenbach et al. (2012) and highlight the sensitivity in the deviation corresponding to an arbitrarily chosen variability of a_r of $\pm 10\%$ and $t_\phi = 1.5 \pm 0.5$ months. This already shifts the mean Ca^{2+} level by about 15 ppb, which is in the same order of magnitude as the long-term trends of around ± 50 ppb found in previous studies (Wagenbach et al., 1996) and also in the core investigated here. The potential variability in the Ca^{2+}-seasonality due to the episodic input of Saharan dust can add a substantial contribution to the deviation (cf. dashed lines in Figure A3). However, the influence of a single Saharan dust event is rather short-term in comparison to the envisaged systematic shifts to a_r and t_ϕ imposed by atmospheric temperature change.

Table A1. Absolute age horizons used in datings of KCC and KCI

Horizon	Year AD	Depth KCC [m WE]	Depth KCI [m WE]
Dust	1977	8.8	4.7
Tritium	1963	11.2	5.8
Dust	1947	15.3	7.7
Dust	1901/02	22.2	11.5

Table A2. Radiocarbon ages used in datings of KCC and KCI

Core	Depth] [m WE]	^{14}C cal [yr b1950]	^{14}C cal sigma [yrs]
KCC	38.5	736	349
	39.2	899	695
	40.9	555	179
	41.3	1007	167
	42.6	1395	300
	43.1	1405	27
KCI	26	365	200
	28.4	1217	336
	30	354	214
	33.9	647	242
	36.2	850	276
	38.5	1178	179
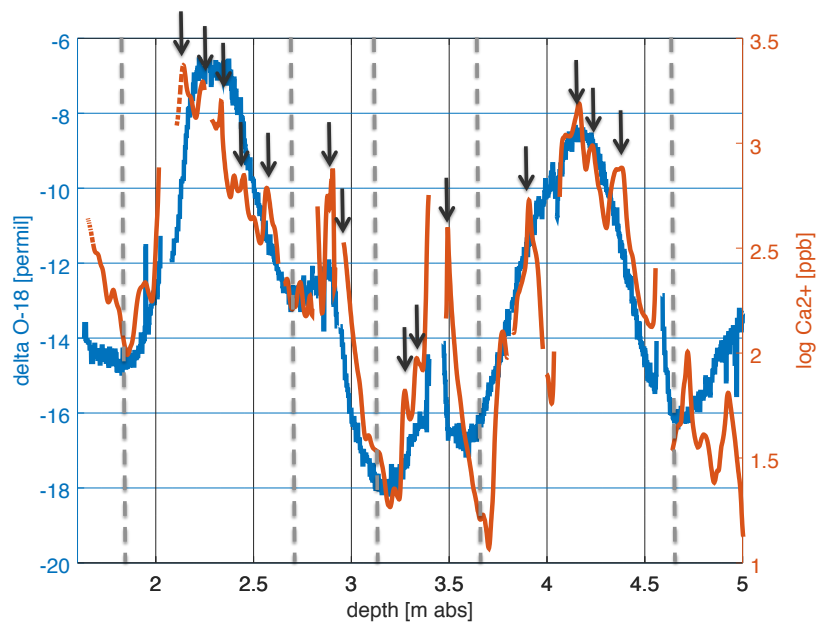
Figure A1. KCC δ^{18}O and Ca^{2+} data shown for the uppermost core section (the first 1.6 m were excavated by a snow trench for drilling). The vertical grey dashed lines indicate individual annual layers determined based on the NH$_4^+$ profile. Black arrows show multiple sub-seasonal local maxima in the Ca^{2+} concentration, supporting the notion of "grouped peaks" revealed by the high resolution LA-ICP-MS Ca profile at greater depths.
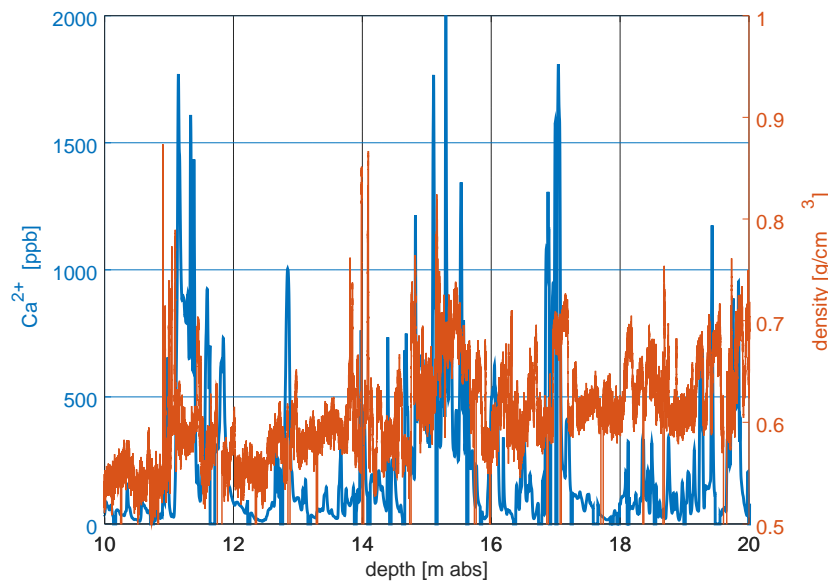
Figure A2. Example view on comparing the KCC Ca^{2+} record with the density profile. Density was measured at high resolution by computer tomography at the Alfred Wegener Institute Bremerhaven (pers. comm. Johannes Freitag). The comparison illustrates the connection between dust content and presumed faster snow preservation: Layers of high dust load coincide with layers of enhanced density (with respect to ambient layers).
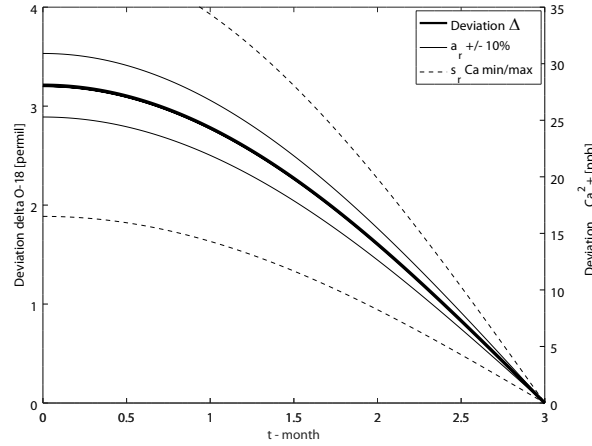
Figure A3. Sensitivity of the average Ca^{2+} signal to snow preservation effects, in comparison to δ^{18}O. The plot shows the deviation of the mean annual ice core signal from the respective precipitation mean as a function of phase shift t between the seasonal cycles of the signal and the accumulation rate. The thick solid black line shows the deviation for δ^{18}O (from Wagenbach et al. (2012)) and Ca^{2+}, plotted on the y-axes on the left and right axis, respectively, and using typical seasonality parameters at Colle Gnifetti (see text). Indicated as thin lines are ranges corresponding to a variability of the relative seasonal amplitude a_r of 10% (arbitarily chosen), and using the estimated maximum uncertainty range of s_r for Ca^{2+} (solid and dashed lines, respectively).